Theoretical Study of the Mechanism for the Markovnikov Addition of Imidazole to Vinyl Acetate Catalyzed by the Ionic Liquid [bmIm]OH

Hui Sun, Dongju Zhang,* Fang Wang, and Chengbu Liu

Key Lab of Colloid and Interface Chemistry, Ministry of Education, School of Chemistry and Chemical Engineering, Shandong University, Jinan, 250100, People's Republic of China

Received: February 3, 2007; In Final Form: March 14, 2007

By performing density functional theory calculations, we have studied the Markovnikov addition of imidazole to vinyl acetate catalyzed by 1-butyl-3-methylimidazolium hydroxide, [bmIm]OH, a novel basic ionic liquid. The purpose is to show the detailed reaction mechanism, to rationalize the experimental observations, and in particular to better understand the role of [bmIm]OH played in the reaction as a catalyst. Two different reaction pathways (stepwise and concerted) have been charactered and analyzed in detail. It was found that both the cation and anion of [bmIm]OH play important roles in the Markovnikov addition, which decrease the barrier and increase the selectivity of Markovnikov addition. The present results rationalize the early experimental findings well and provide a prototype for theoretically understanding the Markovnikov addition catalyzed by room-temperature ionic liquids.

1. Introduction

Since the first air- and water-stable low melting salt, 1-ethyl-3-methylimidazolium tetrafluoroborate ([emIm][BF_4]), was found in 1992,[1] significant progress has been achieved in the study of room-temperature ionic liquids (RTILs). The typical RTILs generally consist of organic cations and inorganic anions, and they exhibit many unique properties,[2−4] including wide liquid range, high thermal stability, powerful solvent capacity, nonflammability, nonvolatility, and good reusability. Moreover, their properties can be varied to some extent for specific applications by changing the anions, cations, or alkyl substituents on the cations. Initially, RTILs were used as environmentally benign reaction media instead of traditional volatile organic solvents because of their negligible vapor pressures and favorable solvation properties.[5−6] However, today much attention has been focused on their significant roles in controlling various organic reactions not only as solvents but also as catalysts.[7−8] So far, a variety of RTILs have been successfully applied in many important chemical reactions such as Friedel−Crafts acylation,[9] Michael addition,[10] and conjugate addition.[11] A good guide for the application of RTILs in synthesis has been published recently by Wasserscheid and Welton.[12] In various RTILs, imidazolium-based RTILs present rapidly increasing importance in the area of catalysis. A number of chemical reactions catalyzed by various task-specific dialkylimidazolium ionic liquids have been reported.[13−16] Although a large amount of experimental works have been carried out to understand the effects of RTILs on chemical reactions, our understanding of how RTILs control desired reactions is very limited. To complement the experimental studies, we have launched a theoretical project of primary researches on the important organic synthesis reactions catalyzed by RTILs based on quantum chemical methods, and the first research prototype has been reported elsewhere.[17]

The N-hetero Markovnikov addition is a powerful reaction for synthesizing organic compounds with carbon−nitrogen linkage and has wide applications in organic and pharmaceutical synthesis. It was traditionally performed under conditions of harsh base,[18−19] strong acid,[20]or high temperature,[21] which often led to environmentally hazardous residues and undesirable byproducts. Recently, some acylases were found to catalyze this reaction;[22−23] however, the procedures were also not free from disadvantages. More recently, Xu et al.[24−25] reported the Markovnikov addition of N-heterocycles to vinyl esters in several RTILs, i.e., 1-butyl-3-methylimidazolium (bmIm) salts, including [bmIm]PF_6, [bmIm]BF_4, and [bmIm]OH. They found that (i) in the presence of [bmIm]BF_4 and [bmIm]OH, the reaction had high selectivity, improved conversion and restrained byproduct, and the reaction time was shorten and the recycle times of catalysts increased; (ii) the reaction did not proceed either without the presence of [bmIm]BF_4 and [bmIm]OH or replacing them by some molecular solvents such as THF, DMF and DMSO; and (iii) no reaction was observed in the ionic liquid containing a PF_6^- anion. These facts demonstrate that bmIm salts generally present excellent catalytic activity for the Markovnikov addition; however, [bmIm]PF_6 is an exception, which was attributed to the poor solubility of N-heterocycles in the [bmIm]PF_6. To better understand the Markovnikov additions promoted by bmIm salts, Xu et al.[25] has proposed a mechanism for the reaction in the presence of [bmIm]OH, which was found to be more effective for catalyzing the desired reaction than [bmIm]BF_4. As shown in Sheme 1, two steps proceed in turn, (i) hydroxyl anion first deprives the N-proton of imidazole and the N atom carrying partial negative charge attacks the partial positively charged α-C atom of vinyl acetate (the carbonyl group in vinyl acetate effectively polarizes the C═C bond), and (ii) the formed H_2O would deliver a proton to the partial negatively charged β-C to obtain the Markovnikov adduct. However, the details of the mechanism are ambiguous and worthy of further exploration. Herein, we consider the Markovnikov addition of imidazole to vinyl acetate in the presence of [bmIm]OH as the second prototype of our systemic studies about the important chemical reactions catalyzed by

* Corresponding author. Email: zhangdj@sdu.edu.cn.

10.1021/jp070962t CCC: $37.00
Published on Web 04/25/2007

SCHEME 1: Proposed Mechanism in the Literature[25] for the Markovnikov Addition of N-Heterocycles to Vinyl Esters Catalyzed by [bmIm]OH

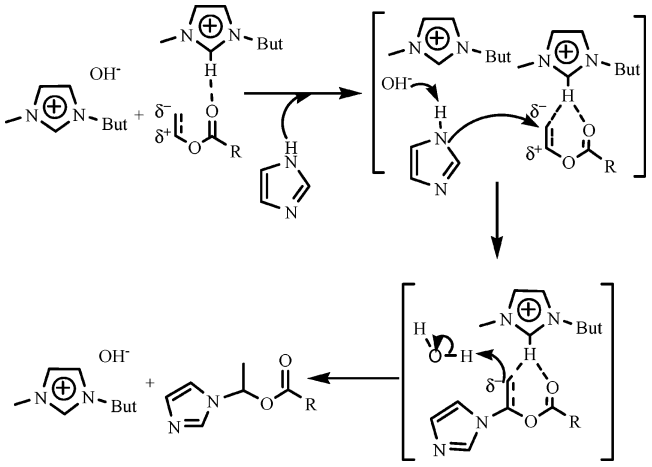

RTILs, and show the detailed reaction mechanism and rationalize the experimental observations by performing quantum chemical calculations.

2. Computational Details

It is well-known that density functional theory (DFT) method[26−29] seems to be an excellent compromise between computational cost and accuracy of the computational outcomes. It has been established in previous researches[30] that hybrid functionals are generally accurate enough to describe the complexes involving strongly bound ionic hydrogen-bonds. In particular, the B3PW91 functional[29,31] has been proven to give the more reliable intermolecular interaction energy than other functionals such as the most popular B3LYP functional. Considering the wide existence of strongly bound ionic hydrogen-bonds in RTILs,[32−36] our calculations were carried out using the B3PW91 functional with 6-311G basis set for all atoms. Polarization functions were added to all the N and O atoms as well as the C atoms of C═C bond in vinyl acetate and the H atoms involved in the hydrogen bonds, and the chosen orbital exponents for N, O, C, and H atoms are 0.864, 1.154, 0.600, and 1.100, respectively. All geometries for the isolated reactants, products, possible intermediates and transition states involved in the Markovnikov addition have been fully optimized without any symmetry constraints. The natures of all the stationary points have been characterized as the local minima or the first-order saddle points by performing frequency calculations, from which the zero-point energies (ZPEs) were derived. The intrinsic reaction coordinate (IRC)[37] pathways have been traced in order to verify that each saddle point links two desired minima. The electronic properties and bonding characteristics for the relevant stationary points were illustrated based on the natural bond orbital (NBO) analysis.[38−39] All calculations were carried out using Gaussian 03 program package.[40] For all the cited energies, the ZPE corrections have been taken into account.

It should be noticed that our calculations were performed using a model of gas phase, which is different from the real ionic liquid condition. In this sense, we only expect that the conclusions derived from the present calculations explain qualitatively the experimental findings.

3. Results and Discussion

On the basis of the computational results, we summarize the reaction process for the Markovnikov addition in Scheme 2.

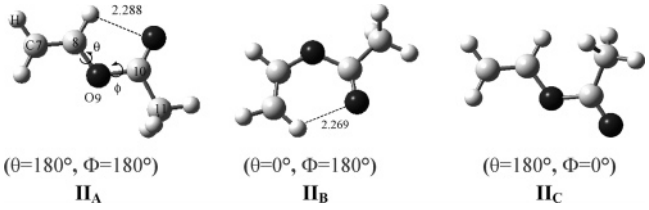

Figure 1. Geometries for three isomers of Vinyl acetate. Distances are in Å. The values in parentheses denote the dihedral angles of $D_{C7-C8-O9-C10}$ (θ) and $D_{C8-O9-C10-C11}$ (Φ).

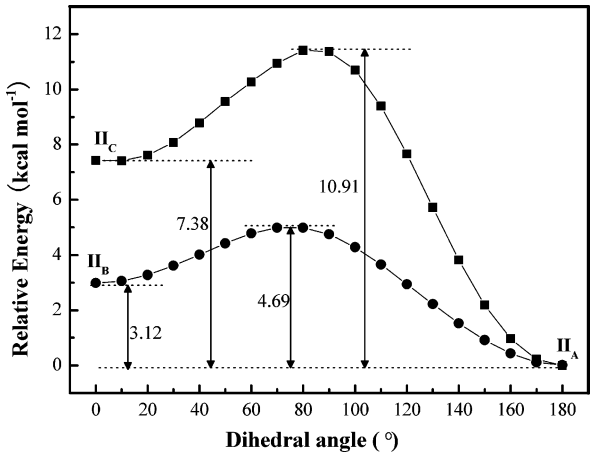

Figure 2. Potential energy surface profiles for the transitions from $\mathbf{II_A}$ to $\mathbf{II_B}$ or $\mathbf{II_C}$ along the dihedral angle $D_{C7-C8-O9-C10}$ (●) or $D_{C8-O9-C10-C11}$ (■), respectively.

For the sake of convenience and clarity, we denote imidazole, vinyl acetate and addition product as **I**, **II**, and **III**, while their corresponding adducts with OH^-, $[bmIm]^+$ and [bmIm]OH are expressed as **I***, **II***, and **III***, respectively. Numbering system of atoms for the reactants is also shown in Scheme 2; thus, the structures and charge distributions on atoms for the species involved in the reaction can be compared with each other. We first inspected the structure of **II** and found that it could exist in three different configurations, $\mathbf{II_A}$, $\mathbf{II_B}$, and $\mathbf{II_C}$, as shown in Figure 1. In Scheme 1, $\mathbf{II_B}$ was used to illustrate the reaction mechanism; however, our computations predict that $\mathbf{II_A}$ is the energetically most favorable isomer. This result is in agreement with the previous works[41−42] on this molecule. From the present calculations, $\mathbf{II_A}$ is 3.12 and 7.38 kcal mol^{-1} more stable than $\mathbf{II_B}$ and $\mathbf{II_C}$. To provide a clear profile for the transitions between the three different configurations, we performed relaxed potential energy surface (PES) scans along dihedral angles $D_{C7-C8-O9-C10}$ (θ) and $D_{C8-O9-C10-C11}$ (Φ), respectively. $\mathbf{II_A}$ was regarded as the initial configuration, and the dihedral angles of θ and Φ in $\mathbf{II_A}$ was set as 180°. During scans, all the degrees of freedom were relaxed except that the dihedral angles of θ and Φ increased with a step of 10° at a range of 0−180°, respectively. So-obtained PES profiles were shown in Figure 2. It can be found that the barriers for conversion of $\mathbf{II_A}$ to $\mathbf{II_B}$ and $\mathbf{II_C}$ are 4.69 and 10.91 kcal mol^{-1}, respectively. The higher stabilities of $\mathbf{II_A}$ and $\mathbf{II_B}$ can be attributed to their effective intramolecular hydrogen bonds (Figure 1). In the present work, both $\mathbf{II_A}$ and $\mathbf{II_B}$ will be considered as appropriate configurations for the Markovnikov addition of **I**, while $\mathbf{II_C}$, in that intramolecular H-bond is absent, is not further considered due to its larger energy demand. From the present calculations, we found that the mechanisms from $\mathbf{II_A}$ and $\mathbf{II_B}$ are slightly different, which will be denoted as pathways **A** and **B**, respectively.

SCHEME 2: Mechanism Details for the Markovnikov Addition of Imidazole to Vinyl Acetate Catalyzed by [bmIm]OH, Proposed from the Present Calculations

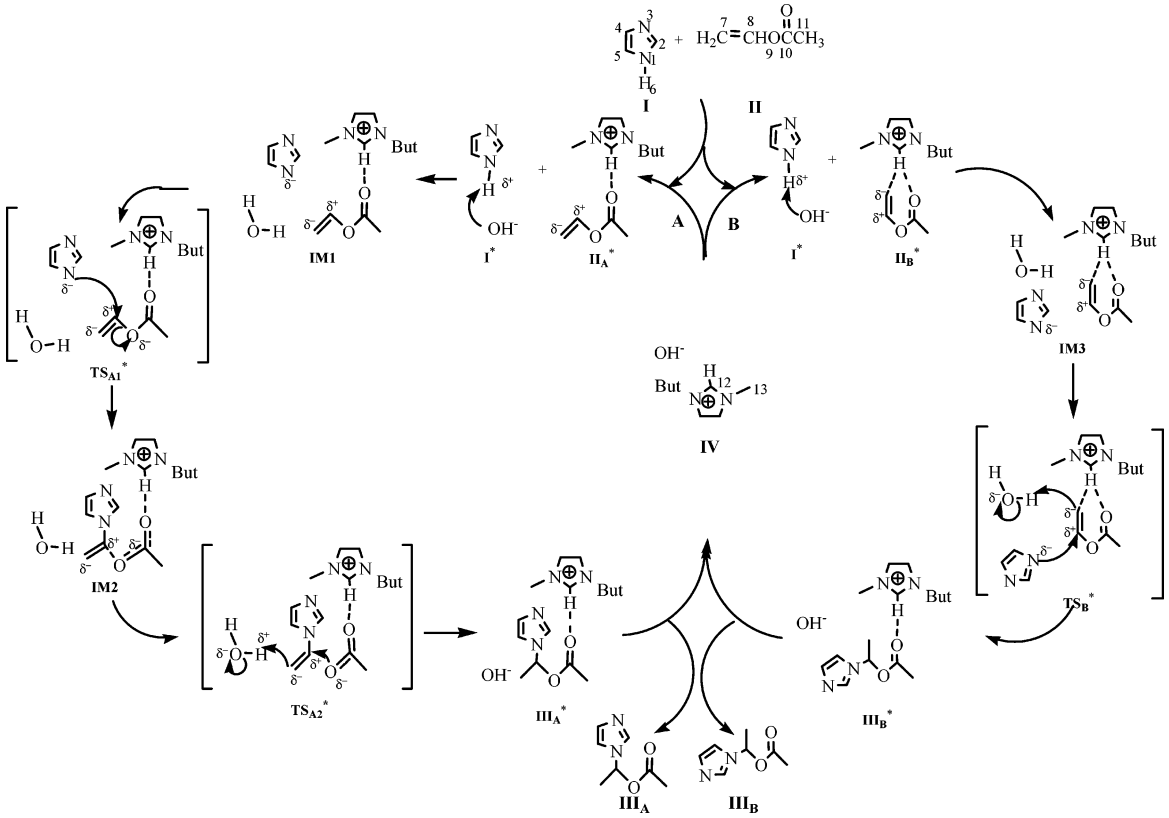

3.1. Reaction Mechanism. Scheme 1 provides us a useful guidance for studying the mechanism of the Markovnikov addition of **I** to **II** catalyzed by [bmIm]OH. We modeled the catalysis of [bmIm]OH on the Markovnikov addition by considering the formation of hydrogen-bonds between the carbonyl oxygen atom of **II** and the hydrogen atoms of $[bmIm]^+$ and the interaction between OH^- and the N1-proton of **I**. Figure 3 shows the most stable structures for **I*** and **II***, respectively.

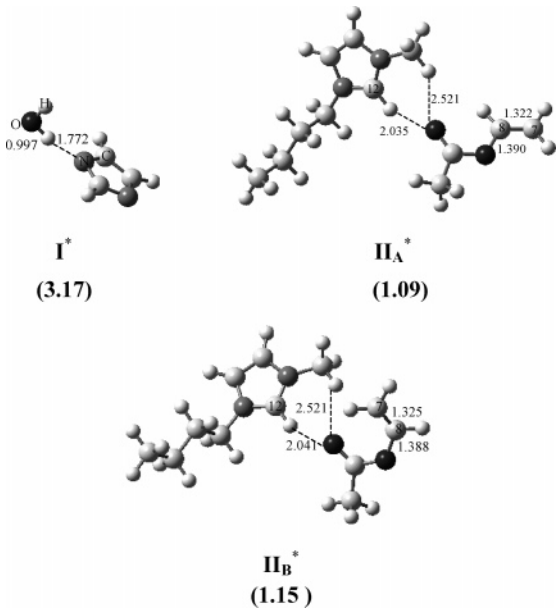

Figure 3. Optimized geometries for dimolecular complexes of imidazole anion$-H_2O$ and vinyl acetate$-[bmIm]^+$. Distances are in Å. The values in parentheses denote the BSSE correction energy (kcal mol^{-1}).

It should be noted that in **I*** the N1 proton of **I** has been deprived by OH^- to form an imidazole anion$-H_2O$ complex. This process is calculated to be exothermic by 78.09 kcal mol^{-1} with regard to the isolated reactants, indicating that the proton migration is an energetically very favorable process. $\mathbf{II_A}$* and $\mathbf{II_B}$* are the complexes of $\mathbf{II_A}$ and $\mathbf{II_B}$ with $[bmIm]^+$ formed via hydrogen bond interactions, where the lengths of the hydrogen bonds are 2.035 and 2.521 Å in $\mathbf{II_A}$*, and 2.041 and 2.521 Å in $\mathbf{II_B}$*. Obviously, the hydrogen bond on C12−H atom is more effective than the other for stabilizing these two complexes. The similar results have been observed in previous theoretical and experimental studies.[32−36] In addition, it is noteworthy that C7 atom in $\mathbf{II_B}$ is much closer to $[bmIm]^+$ than that in $\mathbf{II_A}$. This is favorable for the negative charge transfer at C7 atom to $[bmIm]^+$. $\mathbf{II_A}$* and $\mathbf{II_B}$* are calculated to be 15.50 and 15.67 kcal mol^{-1} more stable than free $\mathbf{II_A}$ or $\mathbf{II_B}$ and $[bmIm]^+$, suggesting their formations are energetically favorable. Moreover, the basis set superposition errors (BSSEs) for these three double-molecular complexes have been estimated using the counterpoise method.[43] The calculated results show that the largest BSSE correction energy is about 3 kcal mol^{-1} (Figure 3), which is much less than the released energies for bringing the two isolate species together to form the corresponding supermolecules. This fact indicates that the neglect of BSSEs in the present study will not change the profile of the PES.

Starting from **I*** and **II***, we have performed detailed PES scans along two pathways, **A** and **B**. The geometries of intermediates and transition states involved in these two pathways have been located and shown in Figures 4 and 5, respectively. The PES profiles along pathways **A** and **B** are depicted in Figure 6, where the sum of the energies of the isolated reactants ($\mathbf{I} + \mathbf{II_A}$ + [bmIm]OH) is taken as zero energy. Our calculations indicate that the mechanisms along paths **A** and **B** are slightly different from each other.

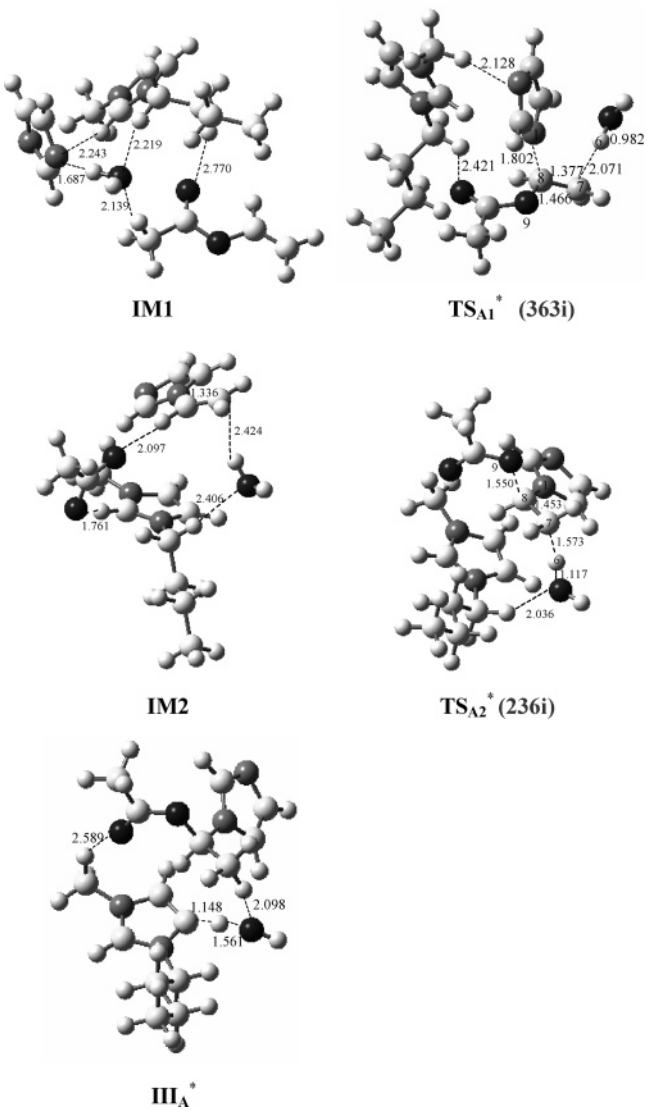

Figure 4. Geometries for intermediates and transition states involved in pathway **A**. Distances are in Å. The values in parentheses denote the imaginary frequencies of transition states.

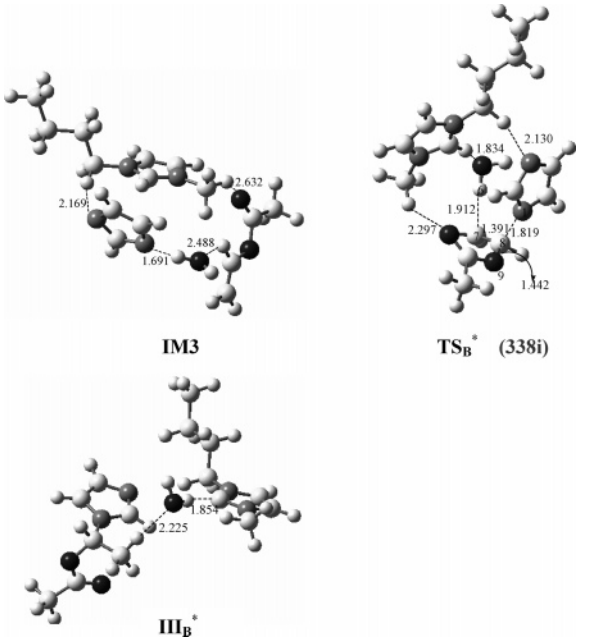

Figure 5. Geometries for intermediates and transition states involved in pathway **B**. Distances are in Å. The value in parentheses denotes the imaginary frequency of transition state.

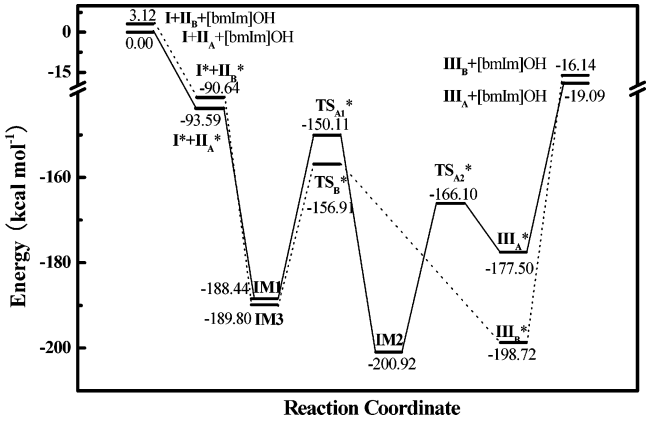

Figure 6. Potential energy surface profiles for the Markovnikov addition along reaction pathways **A** and **B**. The profile linked by solid lines is for pathway **A**, and this linked by dot lines is for pathway **B**.

As shown in Figure 6, pathway **A** involves a stepwise mechanism. Initially, the presence of an electron-withdrawing carbonyl group in $\mathbf{II_A}$ leads C8 atom of vinyl group to carry partial positive charge. The addition reaction is initiated by nucleophilic attack of N1 atom in the imidazole anion to C8 atom via transition state $\mathbf{TS_{A1}}$* (Figure 4). In $\mathbf{TS_{A1}}$*, N1−C8 and H6−C7 distances are 1.802 and 2.071 Å, respectively, while C7−C8 bond length is 1.377 Å, which is 0.055 Å longer than that in the initial dimolecular complex $\mathbf{II_A}$*. Furthermore, we found that C8−O9 distance in $\mathbf{TS_{A1}}$* is longer by 0.076 Å than that in $\mathbf{II_A}$*. The unique imaginary frequency of $\mathbf{TS_{A1}}$* is 363i cm^{-1}, and the corresponding transition vector is mostly associated with the addition of N1 to C8 atom. IRC calculations indicate that $\mathbf{TS_{A1}}$* connects intermediates **IM1** and **IM2**. The instability of the carbanion may be responsible for the formation of **IM2**. The formation of N1−C8 bond causes the extension of C7−C8 bond from double to single bond and hence results in the change of hybridization state of C7 atom. As a consequence, the negative charge on C7 atom increases, which is unfavorable for stabilizing $\mathbf{TS_{A1}}$*. However, the breaking of C8−O9 bond before H6−C7 bond formation can effectively reduce the negative charge on C7 atom, resulting in the formation of **IM2**. The $\mathbf{TS_{A1}}$* was located to be 150.11 kcal mol^{-1} lower than the isolated reactants and 38.33 kcal mol^{-1} higher than **IM1** (Figure 6), while the formation of **IM2** is exothermic by 200.92 kcal mol^{-1} compared with the isolated reactants. Because of the great thermodynamic driving force, the addition reaction is pushed again to form a product-like intermediate ($\mathbf{III_A}$*) via a saddle-point $\mathbf{TS_{A2}}$* with a low barrier, lying 15.99 kcal mol^{-1} lower in energy than $\mathbf{TS_{A1}}$*. The geometry of $\mathbf{TS_{A2}}$* is shown in Figure 4. Distinctly, in $\mathbf{TS_{A2}}$* the N1−C8 bond has almost formed. The dominant motion corresponding to the imaginary frequency mode is the addition of H6 and O9 to C7 and C8, and the lengths of H6−C7 and C8−O9 bond are 1.573 and 1.550 Å, respectively. Moreover, C7−C8 distance is longer by 0.076 Å than that in $\mathbf{TS_{A1}}$*, which is much closer to forming a single bond. The imaginary frequency of $\mathbf{TS_{A2}}$* is much lower than the one corresponding to previous transition structure. As depicted in Figure 6, the rate-determining step along pathway **A** is the formation of N1−C8 bond and the cleavage of C8−O9 bond, and the total reaction along this route is found to be highly exothermic and exergonic, indicating that the channel is remarkably thermodynamically favorable.

TABLE 1: Bond Order (BO) of the Forming and Breaking Bonds in the Transition Structures Involved in Pathways A and B

	C7−C8	H1−C7	N1−C8	C8−O9
$\mathbf{TS_{A1}}$*	1.55	0.06	0.51	0.77
$\mathbf{TS_{A2}}$*	1.21	0.34	0.91	0.68
$\mathbf{TS_B}$*	1.50	0.10	0.50	0.83

Along pathway **B**, it is found that the Markovnikov addition proceeds via a concerted mechanism, where N1−C8 and H6−C7 bonds are simultaneously formed. The transition structure $\mathbf{TS_B}$*, with the unique imaginary frequency of 338i cm^{-1}, is quite similar to $\mathbf{TS_{A1}}$* in pathway **A**, as shown by the geometrical parameters in Figure 5. IRC calculations and further optimization of the primary IRC results demonstrate that two minima connected by $\mathbf{TS_B}$* are **IM3** and $\mathbf{II_B}$*. Note that **IM3** is an initial complex between **I*** and $\mathbf{II_A}$* (not between **I*** and $\mathbf{II_B}$*), indicating that conversion of $\mathbf{II_A}$* to $\mathbf{II_B}$* occurs in the reaction course due to the small barrier between them, as mentioned above. $\mathbf{II_B}$* is a product-like intermediate between $\mathbf{III_B}$ and [bmIm]OH, illuminating the adduct is formed directly from the corresponding transition state without involving any other intermediate. This can be due to the fact that C7 atom of $\mathbf{II_B}$ in $\mathbf{TS_B}$* is closer to $[bmIm]^+$ than the one in $\mathbf{TS_{A1}}$*. Therefore, Coulombic attraction between the partial negatively charged C7 atom and $[bmIm]^+$ is dominant for stabilizing $\mathbf{TS_B}$* after the formation of N1−C8 bond, and before H6−C7 bond formation a small quantity of electron density on C7 atom is transferred to the electron-deficient cation. The total reaction is accompanied by the energy release of 201.84 kcal mol^{-1} as for the isolated reactants with a barrier of 32.89 kcal mol^{-1} with respect to **IM3**.

A comparison between two reaction pathways indicates that pathways **A** and **B** compete with each other. The barrier for forming $\mathbf{TS_B}$* in pathway **B** is only less energy-demanding by 5.44 kcal mol^{-1} than that of $\mathbf{TS_{A1}}$* in the rate-determining step of pathway **A**; however, the isolated reactants (**I**+$\mathbf{II_B}$+ [bmIm]-OH) is higher by 3.12 kcal mol^{-1} than the corresponding reactants (**I** + $\mathbf{II_A}$ + [bmIm]OH). And $\mathbf{III_A}$ is found to be the lower energy conformer, but the energy difference between $\mathbf{III_A}$ and $\mathbf{III_B}$ is only 2.95 kcal mol^{-1}. Furthermore, pathway **B** is more exothermic by 24.34 kcal mol^{-1} than pathway **A**. Overall, from a thermodynamic point of view, both pathways **A** and **B** are highly exothermic and exergonic for the separated reactants. Once the addition reaction is initiated, the large drive would make the reaction proceed continually and easily, although they need overcome small barriers. This is consistent with the experimental findings, i.e., the improved yield, high selectivity, and short reaction time of Markovnikov addition.[25] Therefore, the Markovnikov addition may proceed via these two pathways.

3.2. Frontier Molecular Orbital Analysis. In order to better understand the role of [bmIm]OH played in the Markovnikov addition, it is common to make a frontier molecular orbital (FMO) analysis[44−45] from the reactants to the reactant complexes. According to the FMO theory, it is known that the reactivity between two molecules is inversely proportional to the energy difference between the highest occupied molecular orbital (HOMO) (the lowest unoccupied molecular orbital (LUMO)) of one molecule and the LUMO (HOMO) of the other. The smaller the value of the HOMO−LUMO difference is, the more reactive the chemical reaction is. In Figure 7, we show the HOMO and LUMO energy levels of two reactants in the catalyzed and uncatalyzed processes. It is obvious that the energy differences between $HOMO_I$ and $LUMO_{II}$ are smaller than the differences of $HOMO_{II}$ and $LUMO_I$; thus, the Markovnikov addition of **I** to **II** proceeds via the $HOMO_I$ - $LUMO_{II}$ interaction. However, it is also found that the $HOMO_I$ − $LUMO_{II_A}$ and $HOMO_I$ − $LUMO_{II_B}$ differences are as large as 5.9 eV, which may account for the observed difficulty of the direct Markovnikov addition of **I** to **II**. With the presence of [bmIm]OH, the HOMO and LUMO energy levels of **I** and **II** are remarkably changed, as shown in Figure 7. The main HOMO−LUMO interaction still occurs between $HOMO_I$ and $LUMO_{II}$. The $HOMO_{I^*}$ − $LUMO_{II_A{}^*}$ and $HOMO_{I^*}$ − $LUMO_{II_B{}^*}$ differences are reduced to 3.5 eV, implying that the addition reaction takes place easily. This is in good accord with the experimental results.[25] In addition, it is observed that the $HOMO_{I^*}$ − $LUMO_{II_A{}^*}$ difference is nearly the same with the corresponding $HOMO_{I^*}$ − $LUMO_{II_B{}^*}$ difference, indicating that both pathways **A** and **B** are possible for the addition reaction. This is also in agreement with our computational results.

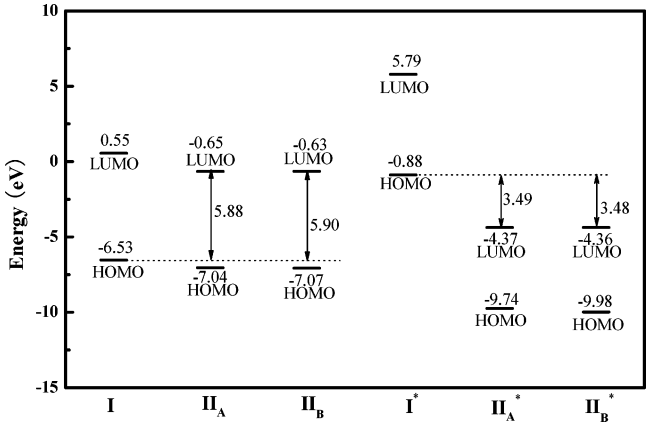

Figure 7. Energies of the HOMOs and LUMOs for imdazole (**I**) and vinyl acetate ($\mathbf{II_A}$ and $\mathbf{II_B}$) in the absence and presence of the catalyst.

3.3. Natural Bond Orbital Analysis. NBO analysis, which can give a better description of the electron distribution and bonding characteristics in compound, has been performed to get more qualitative evidence of the above structural analysis. Table 1 lists bond orders (BO) of the forming and breaking bonds in the transition structures involved in pathways **A** and **B**. Clearly, analysis of the Wiberg bond index matrix[46] in NBO analysis validates these transition structures. BO values of H1−C7 and N1−C8 are 0.06 and 0.51 in $\mathbf{TS_{A1}}$* and 0.10 and 0.50 in $\mathbf{TS_B}$*, showing that N1−C8 bonds are earlier formed than H1−C7 bonds. Moreover, the BO value of C8−O9 bond in

TABLE 2: Calculated Partial Charge and Group Charge from NBO Analyses

	IM1	TS_{A1}*	IM2	TS_{A2}*	III_A*	IM3	TS_B*	III_B*
q(C7)	−0.431	−0.785	−0.481	−0.847	−0.636	−0.422	−0.828	−0.649
q(C8)	0.125	0.242	0.011	0.286	0.331	0.114	0.278	0.332
q(H6)	0.443	0.476	0.476	0.434	0.286	0.498	0.491	0.267
$q(CH_2{=}CH-)$	0.285	0.036	0.191	−0.005	0.293	0.325	0.036	0.312
$q(CH_3COO-)$	−0.300	−0.411	−0.875	−0.451	−0.350	−0.327	−0.374	−0.343
q(imidazole anion)	−0.849	−0.530	−0.209	−0.288	−0.287	−0.849	−0.546	−0.246
$q(OH^-)$	−0.491	−0.506	−0.472	−0.628	−0.778	−0.546	−0.519	−0.550
q([bmIm] cation)	0.911	0.933	0.887	0.937	0.837	0.897	0.913	0.561

$\mathbf{TS_{A1}}$* is less by 0.06 than the corresponding one in $\mathbf{TS_B}$*, indicating C8−O9 bond in $\mathbf{TS_{A1}}$* more inclines to break. In $\mathbf{TS_{A2}}$*, the BO value between N1 and C8 is 0.91, implying that the N1−C8 bond has nearly formed. And BOs of H1−C7 and C8−O9 bonds are 0.34 and 0.68, respectively, indicating that H1−C7 and C8−O9 bonds are forming. These are in good agreement with the structure analysis above.

The charge transfer between reactants is the driving force of a chemical reaction. To further understand the Markovnikov addition, we calculated partial charge and group charge for all the intermediates and transition states, as summarized in Table 2. Evidently, higher charge density is centered on C7 atom relative to C8 atom. This is attributed to the electron-withdrawing effect of the carbonyl group in **II**. Therefore, the central N1 atom of the nucleophilic agent (i.e., imidazole anion) always attacks at C8 atom, which carries less charge density than C7 atom. This is in according with the selectivity of Markovnikov addition. Furthermore, the negative charge on C7 atom in transition states is found to significantly increase with respect to reactants, while the negative charge on imidazole anion remarkably decreases. This is the result of the charge transfer from imidazole anion to C7 atom. In $\mathbf{TS_{A1}}$* and $\mathbf{TS_B}$* the carboxyl group also slightly carries larger negative charge compared to the corresponding reactant-like intermediates **IM1** and **IM3**, and especially in $\mathbf{TS_{A1}}$* the charge density on the carboxyl group more strikingly increases, indicating that the carboxyl group in $\mathbf{TS_{A1}}$* breaks off more easily. While it is noteworthy that the charge density on $[bmIm]^+$ and C7 atom in $\mathbf{TS_{A1}}$* is smaller than those in $\mathbf{TS_B}$*, revealing that the Coulombic attraction between $[bmIm]^+$ and C7 atom in $\mathbf{TS_B}$* is stronger than in $\mathbf{TS_{A1}}$*, as indicated by the smaller distance between them in $\mathbf{TS_B}$*. These facts can rationalize our calculated results: the similar transition structures ($\mathbf{TS_{A1}}$* and $\mathbf{TS_B}$*) lead to different adducts (**IM2** and $\mathbf{II_B}$*).

4. Concluding Remarks

Today RTILs have showed significant roles in controlling many types of reactions as catalysts, although they were initially recognized as alternative green reaction media. However, the catalytic mechanisms of RTILs are generally ambiguous and worthy of exploration. In this paper, the Markovnikov addition of imidazole to vinyl acetate in the presence of the basic ionic liquid [bmIm]OH has been chosen as a prototype of our systemic studies about the important chemical reactions catalyzed by RTILs. Our DFT calculations have shown clearly the catalytic mechanism details of [bmIm]OH controlling the Markovnikov addition as a catalyst. The reaction process has been characterized in detail along two pathways (stepwise and converted). It was found that the Markovnikov addition in the presence of [bmIm]OH is highly exothermic and exergonic. Our calculated results confirm that both the cation and anion of [bmIm]OH have a significant effect on the reactivity of the Markovnikov addition, which has been rationalized via performing the FMO and NBO analyses. $[bmIm]^+$ stabilizes transition state via its Coulombic attraction to C7 atom, while OH^- deprives N1-proton of imidazole to strengthen its nucleophilic ability. The present DFT study explains the experimental findings well and provides a clear profile for the detailed reaction mechanism.

Acknowledgment. This work described in this paper is jointly supported by the National Natural Science Foundations of China (Grant No. 20473047) and the Major State Basic Research Development Programs of China (Grant No. 2004CB719902). We gratefully acknowledge Virtual Laboratory for Computational Chemistry of CNIC and Supercomputing Center of CNIC (Chinese Academy of Sciences), and Shandong University High Performance Computational Center for providing computer resources.

Supporting Information Available: Cartesian coordinates and vibrational frequencies for all species involved (PDF). This material is available free of charge via the Internet at http://pubs.acs.org.

References and Notes

(1) Wilkes, J. S.; Zaworotko, M. J. *J. Chem. Soc., Chem. Commun.* **1992**, *13*, 965−967.
(2) Chiappe, C.; Pieraccini, D. *J. Phys. Org. Chem.* **2005**, *18*, 275−297.
(3) Seddon, K. R. *J. Chem. Technol. Biotechnol.* **1997**, *68*, 351−356.
(4) Jain, N.; Kumar, A.; Chauhan, S.; Chauhan, S. M. S. *Tetrahedron* **2005**, *61*, 1015−1060.
(5) Welton, T. *Chem. Rev.* **1999**, *99*, 2071−2083.
(6) Bourbigou, H. O.; Magna, L. *J. Mol. Catal., A: Chem.* **2002**, *182−183*, 419−437.
(7) Sheldon, R. *Chem. Commun.* **2001**, 2399−2407.
(8) Zhao, D. B.; Wu, M.; Kou, Y.; Min, E. *Catal. Today* **2002**, *74*, 157−189.
(9) Boon, J. A.; Levisky, J. A.; Pflug, J. L.; Wilkes, J. S. *J. Org. Chem.* **1986**, *51*, 480−483.
(10) Yadav, J. S.; Reddy, B. V. S.; Basak, A. K.; Narsaiah, A. V. *Chem. Lett.* **2003**, *32*, 988−989.
(11) Ranu, B. C.; Dey, S. S.; Hajra, A. *Tetrahedron* **2003**, *59*, 2417−2421.
(12) Wasserscheid, P., Welton, T., Eds. In *Ionic Liquids in Synthesis*; Wiley-VCH: Weinheim, Germany, 2003.
(13) Howarth. J.; Hanlon, K.; Fayne, D.; McCormac, P. *Tetrahedron Lett.* **1997**, *38*, 3097−3100.
(14) Park, D. W.; Mun, N. Y.; Kim, K. H.; Kim, I.; Park, S. W. *Catal. Today* **2006**, *115*, 130−133.
(15) Shen, H. Y.; Judeh, Z. M. A.; Ching, C. B. *Tetrahedron Lett.* **2003**, *44*, 981−983.
(16) Ranu. B. C.; Banerjee, S. *J. Org. Chem.* **2005**, *70*, 4517−4519.
(17) Sun, H.; Zhang, D. J.; Ma. C.; Liu, C. B. *Int. J. Quantum Chem.* **2007**, Early View.
(18) Wiley, R. H.; Smith, N. R.; Johnson, D. M.; Moffatt, J. *J. Am. Chem. Soc.* **1955**, *77*, 2572−2573.
(19) Wiley, R. H.; Smith, N. R.; Johnson, D. M.; Moffatt, J. *J. Am. Chem. Soc.* **1954**, *76*, 4933−4935.
(20) Belousov, A. M.; Gareev, G. A.; Kirillova, L. P.; Vereshchagin, L. I. *Zh. Org. Khim.* **1980**, *16*, 2622−2623.
(21) Timokhin, B. V.; Golubin, A. I.; Vysotskaya, O. V.; Kron, V. A.; Oparina, L. A.; Gusarova, N. K.; Trofimov, B. A. *Chem. Heterocycl. Compd.* **2002**, *38*, 981−985.
(22) Wu, W. B.; Wang, N.; Xu, J. M.; Wu, Q.; Lin, X. F. *Chem. Commun.* **2005**, 2348−2350.
(23) Wu, W. B.; Xu, J. M.; Wu, Q.; Lv, D. S.; Lin, X. F. *Adv. Synth. Catal.* **2006**, *348*, 487−492.
(24) Xu, J. M.; Wu, W. B.; Qian, C.; Liu, B. K.; Lin, X. F. *Tetrahedron Lett.* **2006**, *47*, 1555−1558.
(25) Xu, J. M.; Liu, B. K.; Wu, W. B.; Qian, C.; Wu, Q.; Lin, X. F. *J. Org. Chem.* **2006**, *71*, 3991−3993.
(26) Becke, A. D. *Phys. Rev. A* **1988**, *38*, 3098−3100.
(27) Lee, C.; Yang, W. T.; Parr, R. G. *Phys. Rev. B* **1988**, *37*, 785−789.
(28) Perdew, J. P.; Wang, Y. *Phys. Rev. B* **1992**, *45*, 13244−13249.
(29) Becke, A. D. *J. Chem. Phys.* **1993**, *98*, 5648−5652.
(30) Milet, A.; Korona, T.; Moszynski, R.; Kochanski, E. *J. Chem. Phys.* **1999**, *111*, 7727−7735.
(31) Perdew, J. P.; Burke, K.; Wang, Y. *Phys. Rev. B* **1996**, *54*, 16533−16539.
(32) Aggarwal, A.; Lancaster, N. L.; Sethi, A. R.; Welton, T. *Green Chem.* **2002**, *4*, 517−520.
(33) Huang, J. F.; Chen, P. Y.; Sun, I. W.; Wang, S. P. *Inorg. Chim. Acta* **2001**, *320*, 7−11.
(34) Ross, J.; Xiao, J. L. *Chem. Eur. J.* **2003**, *9*, 4900−4906.
(35) Hunt, P. A.; Gould, I. R. *J. Phys. Chem. A* **2006**, *110*, 2269−2282.
(36) Chang, H. C.; Jiang, J. C.; Tsai, W. C.; Chen, G. C.; Lin, S. H. *J. Phys. Chem. B* **2006**, *110*, 3302−3307.
(37) Fukui, K. *J. Phys. Chem.* **1970**, *74*, 4161−4163.
(38) Reed, A. E.; Weinstock, R. B.; Weinhold, F. *J. Chem. Phys.* **1985**, *83*, 735−746.
(39) Reed, A. E.; Curtiss, L. A.; Weinhold, F. *Chem. Rev.* **1988**, *88*, 899−926.

(40) Frisch, M. J.; Trucks, G. W.; Schlegel, H. B.; Scuseria, G. E.; Robb, M. A.; Cheeseman, J. R.; Montgomery, J. A., Jr.; Vreven, T.; Kudin, K. N.; Burant, J. C.; Millam, J. M.; Iyengar, S. S.; Tomasi, J.; Barone, V.; Mennucci, B.; Cossi, M.; Scalmani, G.; Rega, N.; Petersson, G. A.; Nakatsuji, H.; Hada, M.; Ehara, M.; Toyota, K.; Fukuda, R.; Hasegawa, J.; Ishida, M.; Nakajima, T.; Honda, Y.; Kitao, O.; Nakai, H.; Klene, M.; Li, X.; Knox, J. E.; Hratchian, H. P.; Cross, J. B.; Bakken, V.; Adamo, C.; Jaramillo, J.; Gomperts, R.; Stratmann, R. E.; Yazyev, O.; Austin, A. J.; Cammi, R.; Pomelli, C.; Ochterski, J. W.; Ayala, P. Y.; Morokuma, K.; Voth, G. A.; Salvador, P.; Dannenberg, J. J.; Zakrzewski, V. G.; Dapprich, S.; Daniels, A. D.; Strain, M. C.; Farkas, O.; Malick, D. K.; Rabuck, A. D.; Raghavachari, K.; Foresman, J. B.; Ortiz, J. V.; Cui, Q.; Baboul, A. G.; Clifford, S.; Cioslowski, J.; Stefanov, B. B.; Liu, G.; Liashenko, A.; Piskorz, P.; Komaromi, I.; Martin, R. L.; Fox, D. J.; Keith, T.; Al-Laham, M. A.; Peng, C. Y.; Nanayakkara, A.; Challacombe, M.; Gill, P. M. W.; Johnson, B.; Chen, W.; Wong, M. W.; Gonzalez, C.; Pople, J. A. *Gaussian 03*, Revision D.01; Gaussian, Inc.: Wallingford, CT, 2004.

(41) Aroney, M. J.; Bruce, E. A. W.; John, I. G.; Radom, L.; Ritchie, G. L. D. *Aust. J. Chem.* **1976**, *29*, 581−587.

(42) Mora, M. A.; Rubio, M.; Salcedo, R. *Polymer* **1993**, *34*, 5143−5148.

(43) Boys, S. F.; Bernardi, F. *Mol. Phys.* **1970**, *19*, 553−566.

(44) Fukui, K.; Fujimoto, H. *Frontier Orbitals and Reaction Paths: Selected Papers of Kenichi Fukui*; World Scientific: Singapore, 1997.

(45) Hoffmann, R. *Rev. Mod. Phys.* **1988**, *60*, 601−628.

(46) Wiberg, K. B. *Tetrahedron* **1968**, *24*, 1083−1096.